Optimization of Water and Nitrate Use Efficiencies for Almonds Under Micro-Irrigation

Project No.: **12-PREC4-Hopmans**

Project Leader: Jan W. Hopmans
Department of Land, Air and Water Resources
UC Davis
One Shields Avenue
Davis, CA 95616
530.752.3060
jwhopmans@ucdavis.edu

Project Cooperators and Personnel:
Maziar M. Kandelous, Department of LAWR, UC Davis
Patrick Brown, Department of Plant Science, UC Davis
Blake Sanden, Farm Advisor in Kern County, UC Extension

Objectives:

This field study provides critical information on the movement of water and nutrients through the soil under variable soil moisture conditions and provides insight into the interactions of applied irrigation water and nitrogen fertilizer, soil physical properties, soil layering and crop root growth with nutrient use efficiency, and minimizing losses of water (leaching and evaporation) and nitrogen (leaching and denitrification).

The final goal of this research project is to field-validate, optimize, and refine the HYDRUS model under a variety of fertigation regimes using the on-going nutrient study in almonds implemented by P. Brown et al. Results will be used to optimize the management of irrigation and fertigation in an almond orchard. The specific objectives of this project are:

1. To determine optimal irrigation and fertigation practices for micro-irrigation (drip and micro-sprinkler) systems for almond, to improve water and nutrient use efficiencies, and to reduce leaching and gaseous losses of nitrates, using a wide range of possible management scenarios (water, fertigation, salinity);
2. To evaluate the results using the HYDRUS model from extensive field data for specific treatments, and refine it if so needed.

The objectives are achieved by collecting relevant field data such as soil hydraulic and textural properties with soil layering, monitoring of soil moisture and soil water potential, and soil temperature and nitrate solution concentration for selected treatments, in addition to data already being collected as part of the larger nutrient management project. The data collection and analysis is very important since all future model calibration and validation will be based on these data. A final optimization model will provide best management practices for various relevant micro-irrigation layouts with corresponding optimum irrigation and fertigation scheduling for a range of soil types.

Interpretive Summary:

Micro-irrigation methods have proven to be highly effective in achieving the desired crop yields, but there is increasing evidence suggesting the need for the optimization of irrigation scheduling and management, thereby achieving sustainable agricultural practices while minimizing losses of applied water and nutrients at the field scale.

To optimize irrigation/fertigation of almonds, it is essential that irrigation and fertilizers are applied at the optimal concentration, place, and time to ensure maximum root uptake. Moreover, sound and sustainable irrigation systems must maintain a long-term salt balance that minimizes both salinity impacts on crop production and salt leaching to the groundwater. The applied irrigation water and dissolved fertilizer, as well as root growth and associated nutrient and water uptake, interact with soil properties and fertilizer source(s) in a complex manner that cannot easily be resolved with 'experience' and field experimentation alone. It is therefore that state-of-the-art modeling is required with the field observations to allow for unraveling of the most obvious complexities as a result of the typical wide spatial variations of soil texture and layering across farmer-managed fields.

The goal of this research project is to optimize management practices for various micro-irrigation systems for almond, minimizing losses of water (leaching and evaporation), nitrogen (leaching and denitrification), and crop yields by water and salinity stress (droughts). In addition, the applied HYDRUS model with associated root water and nutrient uptake will be evaluated using extensive datasets as acquired from an ongoing nutrient management field project. Therefore, the research project consists of two main components: (a) determining the optimal irrigation and fertigation practices for micro-irrigation (drip and micro-sprinkler) systems for almond, to improve water and nutrient use efficiencies, and to reduce leaching and gaseous losses of fertilizer nitrogen, using a wide range of possible management scenarios (water, fertigation, salinity), and (b) evaluation of the results using the HYDRUS model from extensive field data for specific treatments, and to refine it if needed.

To achieve this goal, this project emphasizes the collection of relevant field data such as soil hydraulic properties, soil texture, and soil layering, and continued monitoring of soil moisture, soil water potential, temperature, salinity, and soil solution nitrate concentration for selected irrigation type treatments. For each of the two irrigation treatments, soil profiles were analyzed to identify soil layers with corresponding textural and hydraulic properties. An extensive set of ECHO-TE soil moisture sensors (Decagon, Inc.), tensiometers, and soil water solution samplers were installed in the tree root zone to monitor the spatial and temporal changes of soil water content, total soil water potential, soil salinity, temperature, and soil solution nitrate. A special tensiometer was designed to monitor and estimate leaching rates of applied irrigation water and nitrate fertilizers.

The 2012-13 annual report focuses on the analysis of field and laboratory measured soil textural and hydraulic properties, with the ultimate goal to assess and evaluate leaching rates of applied water and nitrate fertilizer throughout the year for both irrigation treatments. Much of leaching amounts and rates are largely controlled by irrigation type, soil layering, and applied irrigation water relative to evapotranspiration (ET). The combined installation of tensiometers with solution samplers below the rooting zone are the best way to measure leaching rate.

Although their operating range is limited to relatively wet soils, this is not a limitation as leaching is only relevant if the soil is wet. The main limitation is caused by the large uncertainty of the soil's unsaturated hydraulic conductivity. We recommend using existing databases such as Neuro Multistep as applied in this study, and/or using in-situ soil moisture and soil matric potential data to infer soil hydraulic properties by inverse modeling. Alternatively, we propose to apply a tree-scale water balance technique using spatially-distributed soil moisture measurements to infer field-scale leaching rate and its spatial variations as caused by soil heterogeneity. Tentatively our data suggest that nitrate losses are likely to occur only in the winter and spring period when the soil is wet and root water uptake rates are relatively low.

Materials and Methods:

The presented methods were used for two micro-irrigation systems: drip and fanjet. For each irrigation system, one tree was selected for detailed instrumentation for the purpose of real-time monitoring of soil-water and tree status. The study is part of an ongoing project at Paramount Farms in Lost Hills (near Bakersfield).

Soil Characterization

Among the most important information is an evaluation of the presence of soil layers and the textural/hydraulic properties of each individual layer for typical soil profiles. Using the layering information obtained from soil cores in 2011, we took five undisturbed soil samples (8-cm diameter and 6-cm tall) to measure the hydraulic properties of each identified layer. The constant head method along with multi-step outflow experiment was used to measure the soil water retention curves, saturated hydraulic conductivity, and unsaturated hydraulic conductivity functions for each layer. The multi-step method was introduced by Tuli, et al. (2001) where an initially-saturated soil core is forced to drain by applying a series of positive air pressure steps, while measuring soil core matric potential and drainage outflow volumes during the drainage experiment. The soil hydraulic properties are required to (1) to estimate soil water storage and retention, and (2) to compute leaching rate from the unsaturated hydraulic conductivity using Darcy's equation [Eq. 1]. Also, the bulk density, porosity, saturated water content, and the soil texture of each individual core was determined. However, the multistep method is time-consuming and complicated, thus not conducive for routine measurements.

As it became clear early on that variability of soil texture and layering was large, we collected a total of 160 additional soil samples to a soil depth of 2.5 m at both micro-irrigation treatments. From these the majority of 110 samples were undisturbed samples (either using manual auger or hydraulic giddings) from which either soil bulk density and/or saturated hydraulic conductivity were measured. Rather than using the multi-step method to measure the unsaturated hydraulic properties for each soil sample, we used the neural network approach by Budiman et al. (2004). Based on past soil hydraulic measurements from SJV soils, this so-called Neuro Multistep method allows for prediction of soil hydraulic properties using more easily to obtain soil properties of soil texture, soil bulk density and saturated hydraulic conductivity.

Soil monitoring

Soil moisture and soil water potential. Unfortunately, many of ECHO-5TE (Decagon Inc) soil moisture sensors installed by PureSense in 2011 were useless, because of malfunctioning of sensors and data collection issues. Therefore, we installed a new set-up in 2012. A total of 30 ECHO-5TE (Decagon Inc) soil moisture sensors were installed in the rooting zone of each of the two tree locations in a grid pattern (**Figure 1**), thereby instrumenting one quarter of the tree's rooting zone, at depths of 30, 60, 90, 120 and 150 cm for 6 spatial locations (**Figure 2**). An additional set of sensors were installed at the same depths below the berm in the fanjet plot along the center line (Y-direction) (**Figure 2**). The sensor installation grid was designed such that measurements provide soil information halfway between trees (Y direction), and up to the distance influenced by wetting pattern of either fanjet or drip perpendicular to the trees row (in X direction).

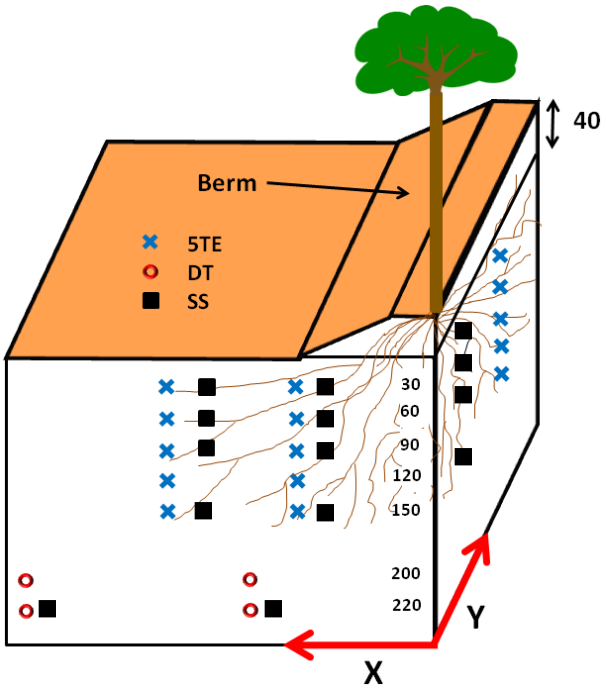

Figure 1. A schematic showing installation depths of various sensor types, with 5TE representing the ECHO-5TE soil moisture, DT the deep tensiometers, and SS referring to soil solution samplers.

The ECHO-5TE provides for measurement of volumetric soil water content, as well as for soil salinity (Electrical Conductivity or EC), and soil temperature. For the purpose of installation, holes were dug with a 5" hand auger. Sensors were provided and are being monitored by PureSense Environmental Inc.

Four pairs of deep tensiometers (red circles) were installed at both fanjet and drip irrigation sites to monitor the total head gradient below the root zone. Two pairs of tensiometers were installed below the canopy where the irrigation water is applied representing the wet part below the root zone and the other two pairs were placed at the middle distance between two tree rows, representing the most dry region for both treatments. In addition, five neutron probe

access tubes were installed in neighboring tree plots (**Figure 2**) for each treatment, allowing for soil moisture and soil water storage measurements to a depth of 2.7 m in 30-cm depth intervals. Neutron probe measurements were collected one day prior to each irrigation. The neutron probe was calibrated using independent gravimetric soil moisture samples using linear regression, with a non-zero intercept (See **Figure 3**).

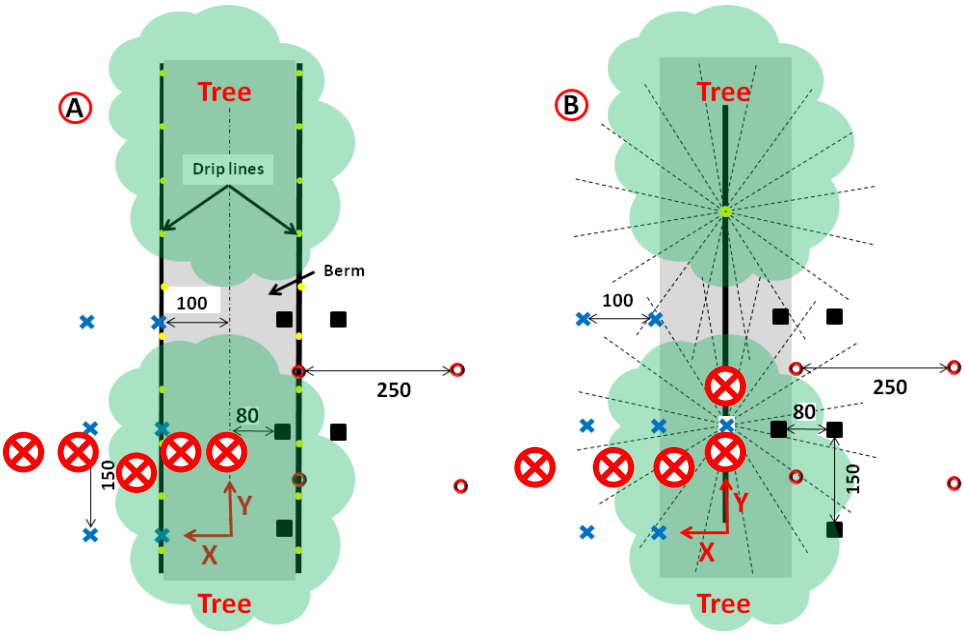

Figure 2. A schematic top view of the installed soil moisture sensors, deep tensiometers, and solution samplers in (A) Drip and (B) Fanjet site. The red crossed circles denote the approximate location for the neutron probe access tubes, blue x's representing the ECHO-5TE soil moisture sensor, small red circles representing deep tensiometers, and black squares referring to the solution soil samplers.

In addition, five neutron probe access tubes were installed in neighboring tree plots (**Figure 2**) for each treatment, allowing for soil moisture and soil water storage measurements to a depth of 2.7 m in 30-cm depth intervals. Neutron probe measurements were collected one day prior to each irrigation. The neutron probe was calibrated using independent gravimetric soil moisture samples using linear regression, with a non-zero intercept (See **Figure 3**).

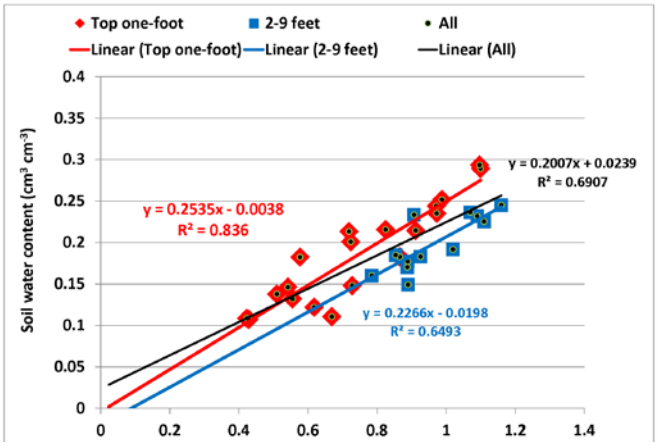

Figure 3. Neutron probe calibration curves for the top one-foot (red diamonds), 2-9 feet (blue squares), and for all data combined (black regression line).

Leaching rate calculations. Leaching rates can be estimated if the hydraulic conductivity and the total head gradient across the soil layer below the root zone are known. The leaching flow rate, q_{AB}, can be calculated using the Darcy equation as follows:

$$q_{AB} = -K(h)\frac{H_B - H_A}{\Delta z_{A-B}} \text{ or } q_{AB} = -K(\theta)\frac{H_B - H_A}{\Delta z_{A-B}} \quad , \qquad \text{[Eq. 1]}$$

where *q* denotes the Darcy water flux (inches day $^{-1}$), *K(h) or K(θ)* represent the unsaturated soil hydraulic conductivity, which is a function of the soil matric potential *h or θ* at the deep measurement depth. In the Darcy equation, H_A and H_B denote the total water head values at bottom and top of the soil layer below the root zone, respectively, and Δz_{A-B} signifies the thickness of the soil layer between the tensiometers. As shown in **Figure 1** the set of deep tensiometers were installed at four different locations at depths of 200 and 220 cm. Using the measured soil matric potential values above and below the impeding layer and its thickness, we computed the total head gradient for each of four individual measurement locations for each site. Using the measured soil water matric potentials and soil water content along with the unsaturated hydraulic conductivity for the soil layer in question, one calculates the leaching rates by multiplying the unsaturated hydraulic conductivity with the total head gradient, according to Eq. [1]. The choice of using either water content or pressure head measurements for the conductivity estimation depends on the accuracy of the measurement and the sensitivity of either of the two variables on the unsaturated hydraulic conductivity value (see Results and Discussion, Soil textural analysis). We used the hydraulic conductivity based on soil matric potential, K(h), as we concluded that the measured soil matric potential measurements with the deep tensiometers were very accurate in the wet soil moisture range.

Deep tensiometer design. Leaching rates require continuous head gradient measurements across the soil layer of interest below the rooting zone. However, the vertical tensiometer length is one of the main factors limiting its operation range. To remove this constraint for deeper soil water tensiometric measurements, we developed a special deep tensiometer that can be operated across the maximum application range (0-850 cm). This was done by installing the pressure transducer at the tensiometer cup, as opposed to conventional tensiometers where the pressure transducer is installed at the soil surface. **Figure 4b** shows the result of laboratory evaluation of the new design for several wetting and drying cycles, including times at which the tensiometer was serviced by refilling with water (blue arrows). The components of this new designed tensiometer are presented in **Figure 4a**.

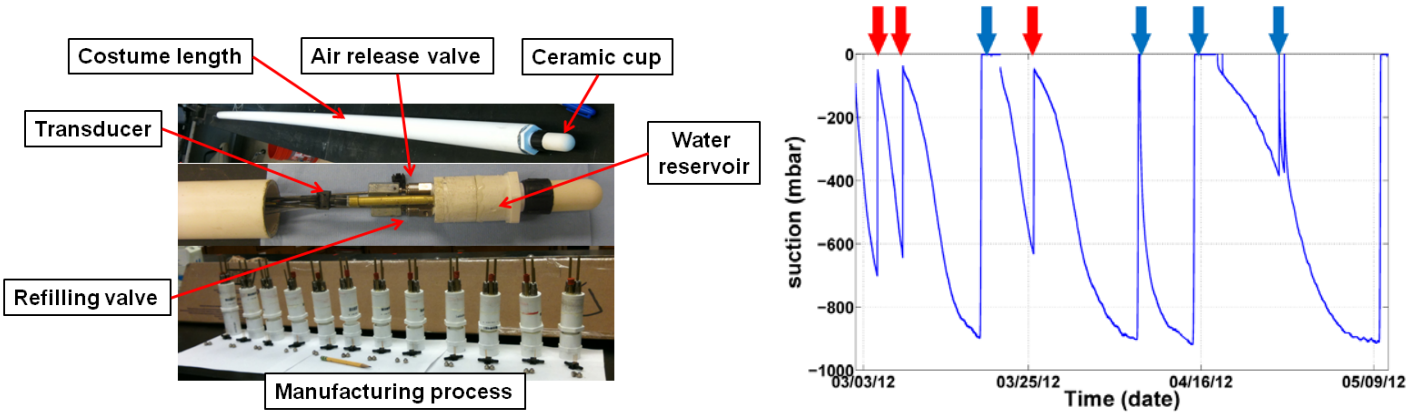

Figure 4. (a - left) Deep tensiometer design and (b - right) Laboratory evaluation of the deep tensiometer during wetting and drying cycles. Red arrows show soil wetting with blue arrows representing times of refilling the tensiometer cup.

We believe this new design is critical for application in irrigated systems requiring tensiometer measurements at large depths below the rooting zone to estimate soil water leaching rates. This new design is being field validated and will be used for measuring the leaching rate in the near future in this and related projects.

Additional Required Input Data for Modeling

In addition to soil physical characterization, other required input data for the HYDRUS modeling includes measurements of tree evapotranspiration (ET), water application rates and spatial distribution for the drip and fanjet systems, fertigation amounts and rates, and tree root distribution. Daily ET rates are available from eddy-covariance data collected at the fanjet site, whereas volumetric flow rates are determined from flow meter measurements installed in the irrigation lines.

Figure 5. Measurement (a and b) of water application uniformity and uniformity pattern (c) for the fan jet (1 hour volume measurements).

The wetted area for the drip system is monitored by visual inspection, whereas the water application uniformity of the fanjet system was determined from measurement of water volumes in 110 10-cm diameter catch cans, distributed within the quarter section of the instrumented fan jet plot (**Figure 5**). Though additional uniformity data will be collected, soil moisture patterns indicate that the measured patterns are consistent during the irrigation season.

Water Balance

In addition to estimation of leaching rates using the Darcy equation from tensiometric measurements [Eq. 1], leaching rates (LR) can be determined from the tree-scale water balance using measurements of applied irrigation water (IW), precipitation (P), tree evapotranspiration (ET), and changes in soil water storage (ΔS) to a specific soil depth below the rooting zone. As the depth of the soil water storage measurements increase, we expect the estimated LR to be more accurate as it would increasingly account for upward capillary rise. Thus, from periodic measurements of ΔS, and corresponding data of IW (flow meter measurements), P (rain gauge), ET (eddy covariance tower) and ΔS (neutron probe), the leaching rate (LR) can be computed from with the measurement unit in depth of water (inches):

$$LR = IW + P - ET - \Delta S \quad , [Eq. 2]$$

Whereas IW, P, and ET are area-wide measurements, we divided the tree plot in two equal size sections representing the tree rooting zone (along the tree rows) and dry zone (section between tree rows), where ΔS from the dry zone was determined from the neutron probe measurements furthest away from the tree row. The amount of water applied through irrigation system (IW) was monitored from flow meters for each site. The water volume delivered to each tree was divided to the area occupied by each tree yielding the equivalent depth of applied irrigation water. The number of dripper (20 drippers of 4 l/hr per tree) designed was such that the amount water delivered to each tree was equal to the amount of water applied to each tree of the fanjet site (2 fanjets of 40 l/hr per tree).

Nitrate Sampling

A total number of 20 shallow soil solution samplers were installed in both fanjet and drip irrigation systems (black square in **Figures 1 and 2**) to monitor the soil root zone nutrient status after each fertigation throughout the year. Additionally four deep solution samplers were installed close to the deep tensiometers to measure the nitrate concentration of leached irrigation water (**Figure 2**). From the measured soil solution nitrate concentration, the mass of leached nitrate can be computed by multiplying nitrate concentration with the soil leaching rate (LR), as computed from **Eq. 1**. For that purpose, the solution nitrate concentration was multiplied by the depth-corresponding soil volumetric water content, thereby converting the mass of nitrate per volume of soil solution to the mass of nitrate per volume of soil.

Soil solution samples were taken the day before and three to four days after each fertigation, by applying a 60-70 cbar vacuum to the solution sampler at the end of the day, after which solution was collected in the morning of the following day. The collected samples were kept cold (under ice) until analyzed in the lab for nitrate concentration measurement using a Shimadzu BioSpec-mini UV/Visible scanning spectrophotometer (540 nm). If periodic measurements of the applied fertilizer N and the amount stored in the tree's biomass (nuts and leaves) are available, then nitrate leaching rates can also be computed from a nitrate mass balance. However, insufficient data were available to conduct such an analysis.

Results and Discussion:

Soil Textural Analysis

Analysis of soil texture for both the fanjet and drip sites showed that the soil profile of the studied almond orchard is highly heterogeneous and layered. **Figure 6** shows representative soil layers and differences of soil profiles between the drip and fanjet site. The top one meter of soil profile at the fanjet site consists of coarse soil material, allowing quick infiltration of applied irrigation water. The profile includes two 20 cm thick fine-textured soil layers at approximate depths of 130 and 200 cm soil depth.

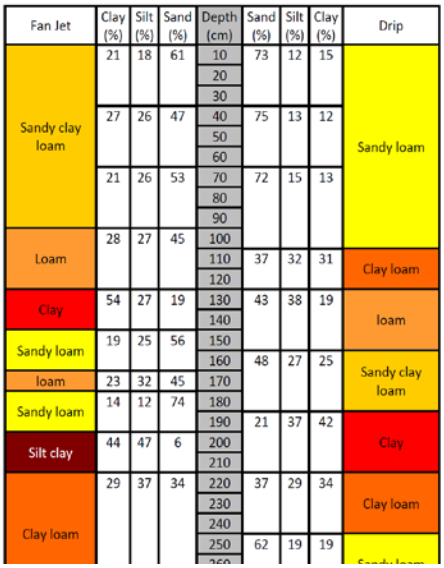

Figure 6. A schematic with soil layers and soil texture for the drip and fanjet sites.

We believe the difference in depths of clay layers between the two irrigation plots has significant implications on leaching rates. These layers will prevent and/or delay downward water movement below the root zone. The drip site shows depth variations in soil texture as well, with the fine-textured soil layer at about the 180 cm.

As we have concluded already, the enormous depth variation in soil texture and soil layers at the tree plot scale introduced large uncertainty of the mean and variation in soil texture and related soil hydraulic properties, thus introducing large uncertainty in specific soil layering depths. However, further soil core sampling at both experimental sites was needed to ascertain the depth variation of soil texture and hydraulic properties and their spatial heterogeneity of soil profiles within and between the two irrigation sites. **Figures 7** and **8** present the spatial heterogeneity of soil properties and layering within and between Drip and Fanjet irrigation sites. Although there are significant variations in soil layering and textural/hydraulic properties, the soil layering follows the same pattern as was identified at the beginning of this project (**Figure 5**). Also, there is consistency in the data, with depth variations in saturated hydraulic conductivity (Ksat), coinciding with either depth variations in soil bulk density or sand/clay content. For example, the clay and clay loam layers in **Figure 6** correspond with soil layers of decreasing Ksat for both the drip (100 and around 200 cm) and fanjet (100 and 180 cm) sites.

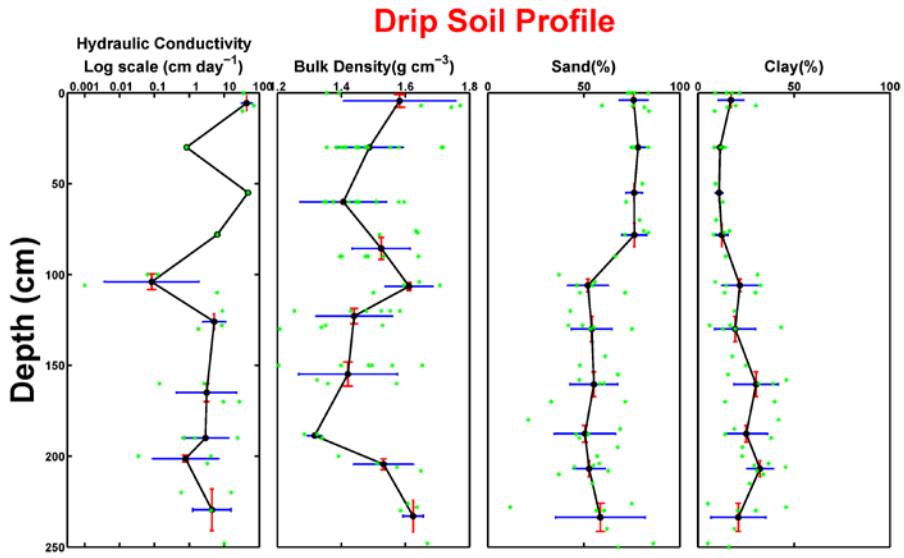

Figure 7. Mean (black line) and standard deviation (blue horizontal lines) values of saturated hydraulic conductivity (Ksat), dry bulk density, sand and clay content as a function of soil depth for the drip site.

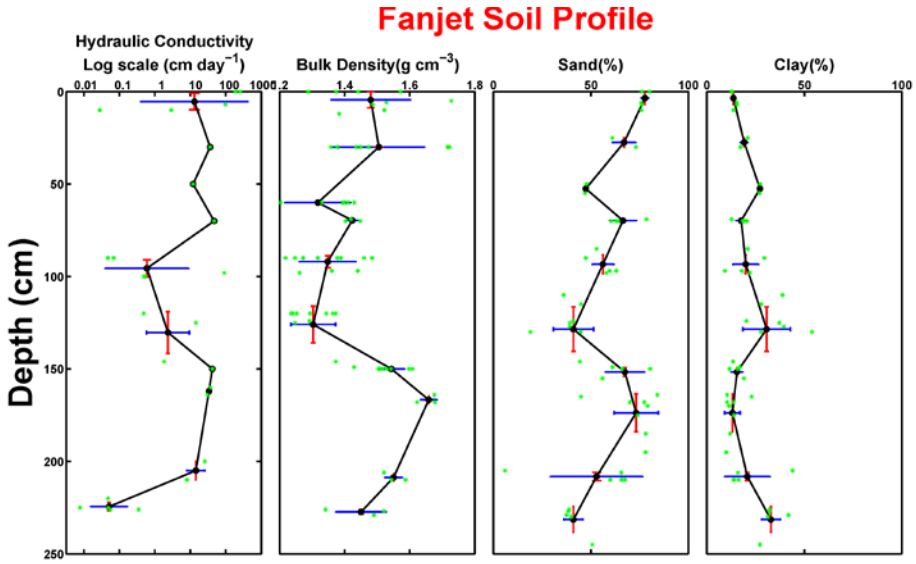

Figure 8. Mean (black line) and standard deviation (blue horizontal lines) values of saturated hydraulic conductivity (Ksat), dry bulk density, sand and clay content as a function of soil depth for the fanjet site.

Soil Hydraulic Properties

Figure 9 shows the soil water retention and unsaturated hydraulic conductivity curves for the five core samples from different soil textural layers (**Table 1**) as measured using the multistep outflow method in the laboratory. The results show the enormous variability of the soil water retention curves, and the resulting uncertainty of the unsaturated hydraulic conductivity (gray areas) if the soil texture at the deep instrumented soil layer is unknown. Though not shown in

this report, we compared the Neuro Multistep predictions with measured hydraulic functions and concluded that the predicted curves agreed fairly well with the measured ones.

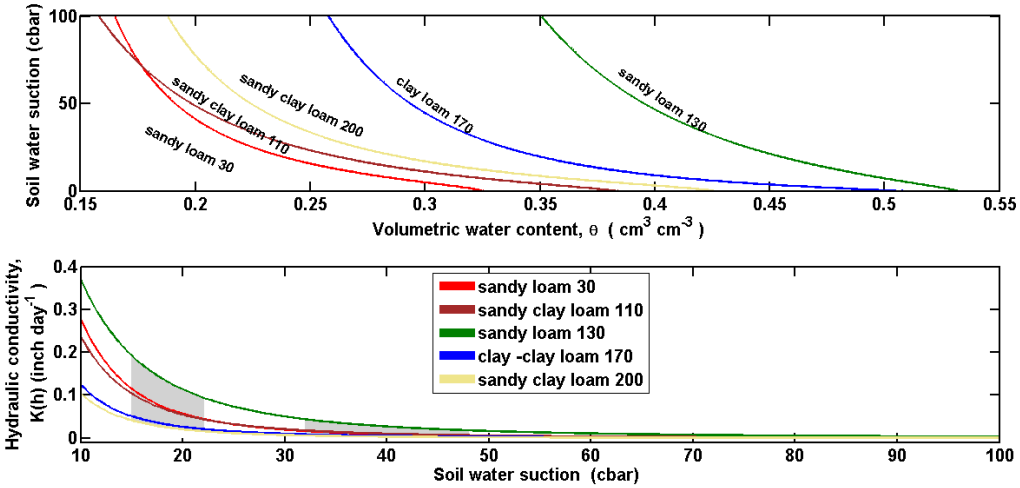

Figure 9. Soil water retention and unsaturated hydraulic conductivity curves for the different soil types. Shaded portions represent the variation in unsaturated hydraulic values as a result of variations in measured soil water pressure head values across the field plot sites.

Table 1. The textural and physical properties of soil samples in **Figure 9**.

Soil #	Sand (%)	Silt(%)	Clay (%)	Ks (Inches/day)	Bulk Density (g/cm^3)
Sandy loam 30	76	10	14	7.68	1.72
Sandy clay loam 110	48	22	30	13.57	1.5
Sandy loam 130	75	12	13	11.89	1.21
Clay – Clay loam 170	33	27	40	41.51	1.16
Sandy clay loam 200	57	20	23	4.23	1.39

Hence, it was decided to apply the Neuro Multistep model to predict both the soil water retention and unsaturated hydraulic conductivity curves using the soil physical data from the collected 21 soil samples (12 samples from drip and 9 samples from fanjet site) of the 200-240 cm depth interval (**Figure 9**).The results are presented in **Figure 10,** with the corresponding soil physical property values used for the prediction in **Table 2.** From the curves in **Figure 10**, it becomes instantly clear that the variation in soil water retention and unsaturated hydraulic conductivity is enormously large, even when considering the 200-240 cm depth interval only. Hence, accurate soil textural information (both mean and variation) of soil textural properties is extremely important to estimate leaching rates and its field-scale variations. Comparing the hydraulic conductivity curve as function of soil water content (θ, bottom panel) with the hydraulic conductivity curve as function of soil matric potential (h, center panel) one readily determines that a small uncertainty in soil water content results in a huge uncertainty in predicted unsaturated hydraulic conductivity. In contrast, when considering a similar size uncertainty in the measured soil matric potential, the uncertainty of the predicted hydraulic conductivity is relatively small. Therefore, when estimating leaching rates (LR) using **Eq. 1**, we will use the K(h) function in concert with soil water matric potential measurements.

Table 2. Soil variation in textural and physical properties for soil samples presented in **Figures 7** and **8** (200-240 soil depth, for 12 samples from drip and 9 samples from fanjet plots).

	Drip					Fanjet				
#	Sand (%)	Silt (%)	Clay (%)	Ksat (in/day)	Bulk density (g/cm^3)	Sand (%)	Silt (%)	Clay (%)	Ksat (in/day)	Bulk density (g/cm^3)
1	52	33	14		1.32	74	24	2	9.98	1.52
2	46	40	14		1.28	66	18	16		1.52
3	48	14	38	9.31	1.34	67	19	14	3.23	1.54
4	65	25	10	0.27	1.60	60	24	16		1.59
5	43	41	16	0.01	1.55	69	19	12	0.02	1.46
6	58	5	37	1.30	1.51	78	19	3	0.02	1.47
7	45	9	46		1.57	39	29	32	0.14	1.34
8	63	7	31		1.65	38	30	32		1.52
9	41	45	14	0.23	1.47	38	21	42		1.49
10	75	20	5		1.61					
11	12	42	46		1.64					
12	57	13	30	1.65	1.58					

Soil Moisture Measurements

To assess the accuracy and uncertainty of the EchoTE-5 soil moisture sensors, we took selected soil samples near the soil surface for a wide range of soil moisture conditions and both irrigation sites and compared those with nearby (within 30 cm distance) sensor measurements. As is shown in **Figure 11**, the soil water content measured with the 5-TE sensors is within about 4% (volumetric water content) of the independently measured soil water content, as determined from the 67% uncertainty band (red dotted lines). We realize that the accuracy is also controlled by spatial soil moisture variations within the sampled 30-cm separation distance as determined by soil variability, sampling error and non-uniform water applications.

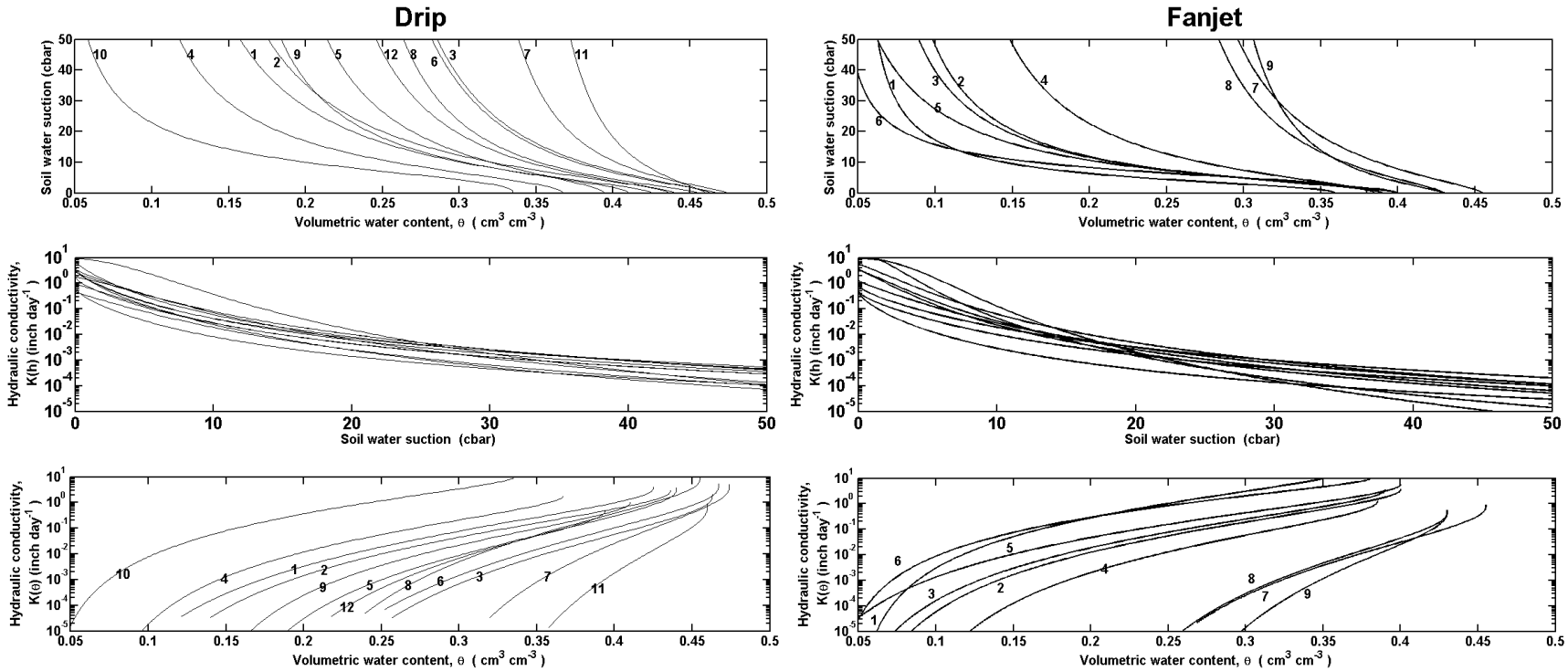

Figure 10. Soil water retention (top panel) and unsaturated hydraulic conductivity curves for the different soil samples taken for the 200-240 depth intervals for both the drip (left) and fanjet (right) sites. The center panel presents the predicted unsaturated hydraulic conductivity curves as function of soil matric potential, whereas the two bottom plots present the unsaturated hydraulic conductivity curves for the same soils, as function of soil water content.

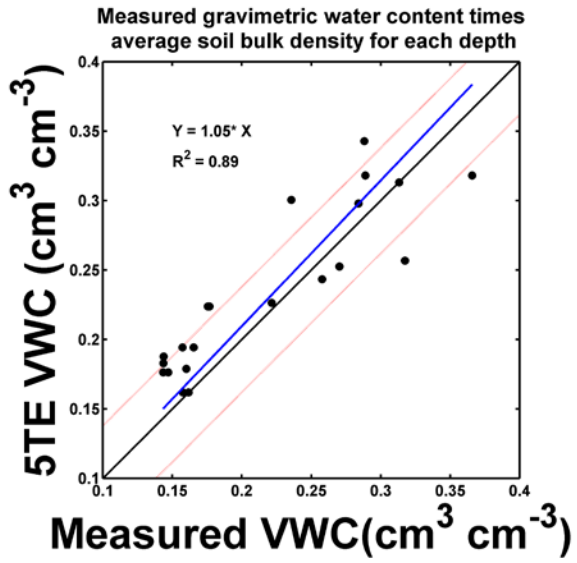

Figure 11. Calibration curve for ECH2O 5-TE water content sensor. Black circles represent the data points, whereas the dotted red lines show the 67% uncertainty band around the 1:1 black line. The blue line is the fitted line by linear regression (R2 = 0.89).

Figures 12 and 13 present the spatial and temporal variation of soil water content in the root zone for the drip and fanjet irrigation site for the new installation setup, respectively, as obtained from the EchoTE-5 real time measurements every half an hour starting April 1, 2012. The pink and blue bars indicate the irrigation and rain events during the presented time period, respectively. The (X, Y) notation represents the Cartesian coordinate system, with both X and Y representing distances (cm) from the tree trunk. For example, the panel with the (0,150) notation presents soil water content data that is exactly along the tree row (X = 0 cm) and midway between the trees (Y = 150 cm). Similar to the 2011 data set, the sensors installed at depths of 30 and 60 (and 90 cm added at 2012) of the drip site (**Figure 12**) respond to the irrigation and precipitation events showing the affected soil profile by the moving wetting front. The mild response of Echo sensors at the 120 and 150 cm soil depth along with their relatively high and constant water content values is a reflection of the perching of water above the 180-220 cm depth clay layer (**Figure 6** and **7**). The spatial variation in soil water content at depths 120 and 150 cm confirm the soil heterogeneity presented in **Figure 7** demonstrating variable-textured soil layers at the tree plot scale. Both the decreasing and constant water content at depths of 120 and 150 cm during the winter season suggest that precipitation amounts were relatively small or was largely intercepted by the tree canopy, since neither shallow sensors responded to those precipitation events. Comparing the minimum soil water content during the growing season and winter, we conclude that the soil water content remains at its lowest level during the winter, thus suggesting that the soil moisture profile was not affected by winter rainfall.

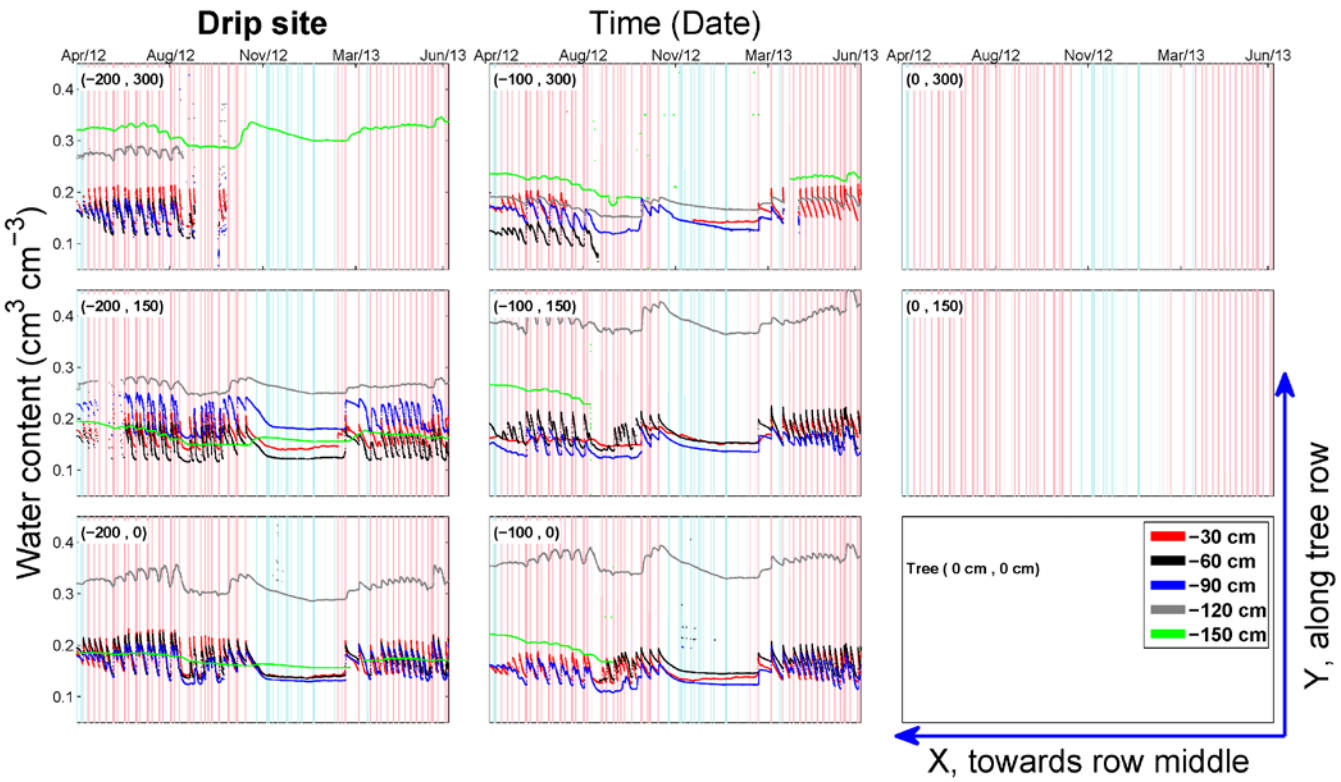

Figure 12. Spatial and temporal variations of soil water content in the root zone under **drip** irrigation system for 2012-13. The pink bars indicate irrigation events and the blue bars denote the precipitation events. The width of each bar represent the duration of each irrigation or precipitation events.

For the fanjet soil moisture measurements of **Figure 13**, the shallow sensors at depths of 30 and 60 cm immediately responded to irrigation events, but to a lesser extent than for the drip irrigation treatment which is due to the larger application area for the fanjet as compared to the drip site. Comparing the temporal variations of water content at depths of 30 and 60 cm for locations (-100, 150) and (-200, 150) between the 2012 and 2013 irrigation seasons shows that the local soil moisture response was much larger, as caused by the installation of a single dripper along the water application line for the purpose of increasing water application rate without increasing irrigation duration. The clay layer at the 120 cm depth (**Figure 5**) is the main reason that there the water content is highest, as caused by the perching infiltrated soil water. Low water content values at the 150 cm soil depth can be explained by reduced leaching across the clay layer with spatial variations caused by the non-uniform water application pattern and soil heterogeneities. In fact, spatial variations in root zone water content can be related to either of water application pattern of **Figure 5** or heterogeneities presented in **Figure 8**.

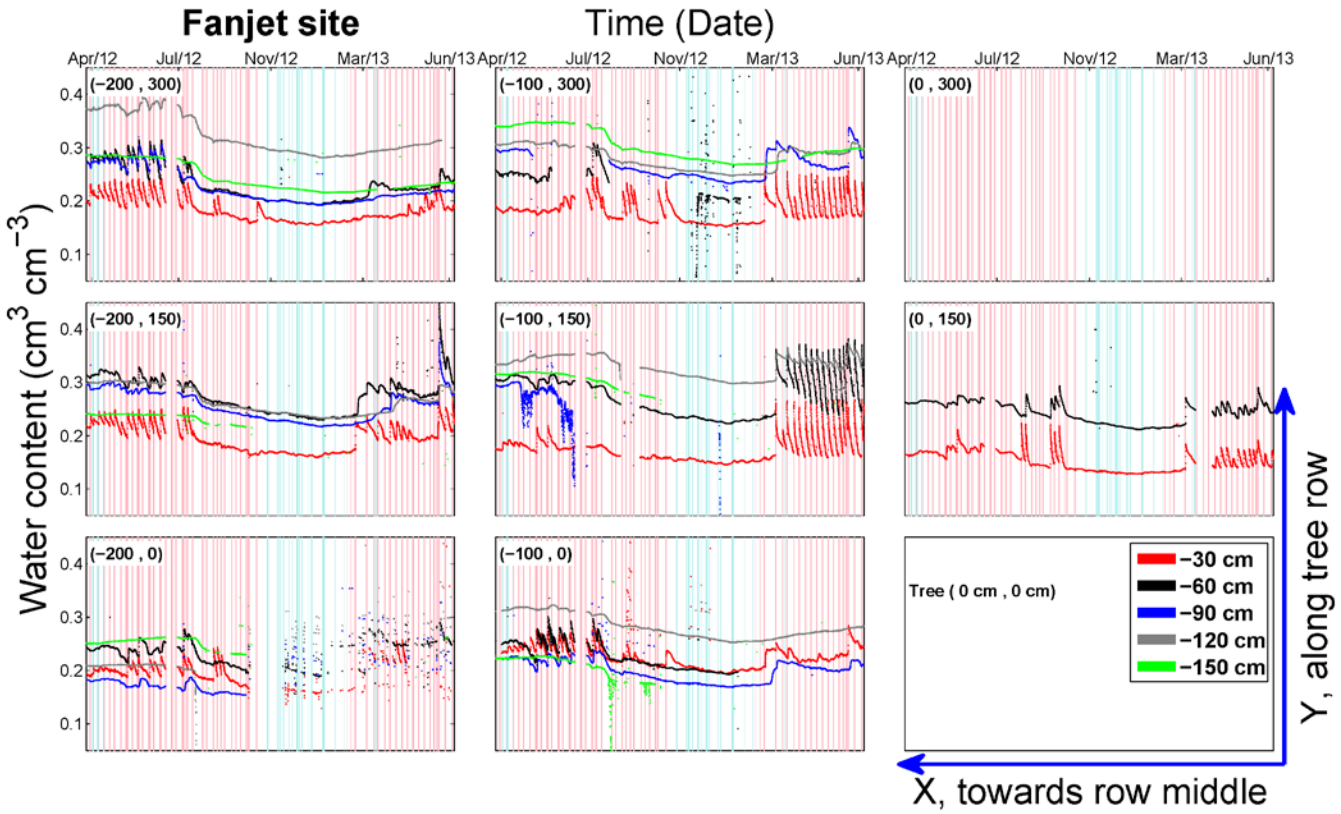

Figure 13. Spatial and temporal variations of soil water content in the root zone under **fanjet** irrigation system for 2012-13. The pink bars indicate irrigation events and the blue bars denote the precipitation events. The width of each bar represent the duration of each irrigation or precipitation events.

Leaching Rate

The amount of water leaching (LR, inches) for both irrigation sites was analyzed using two different approaches. The first method uses the water balance at the tree plot scale from measurements of applied water, evapotranspiration, and soil water storage measurements (see below: Water Balance). In the second approach, we applied Darcy equation [**Eq. 1**], to compute leaching rates from tensiometric soil water potential measurements combined with predicted unsaturated hydraulic conductivity values using the Neuro Multistep method (see below: Darcy Equation). The presented water balance was computed for the 2009-2013 period.

Water Balance[1]**.** Precipitation (P) and Evapotranspiration (ET). **Figure 14** (Left panel) shows the cumulative precipitation data obtained from a nearby CIMIS station (#146) and assumed representative for both irrigation sites. The amount of precipitation in the first two years (late fall 2009 and 2010 and early winter 2010 and 2011) was significantly higher as compared with the last two years, thus resulting in reduced soil water storage for 2011 and 2012 at the start of the irrigation season and expected less likelihood of leaching for those two years.

[1] Most if not all of the data used for this part of our annual report were provided by Blake Sanden, a farm advisor in Kern County, UC Extension Center.

The right panel of **Figure 14** shows the cumulative potential evapotranspiration (ET_o) data obtained from a nearby CIMIS station (blue) and the actual ET (ET_a) Eddy-Covariance tower located in the orchard (red) for four consequence years. The data show that the ET_a / ET_o ratio has been decreasing from greater than one in 2009 to less than one in 2012. Assuming that the crop coefficient was not changed in the potential ET calculations, we believe that the decreasing ET in 2011 and 2012 is caused by lower tree canopy area or leaf area values, as a result of disease, stress or other physiological factors unknown at this time. This will be further investigated by reviewing available leaf area index and yield data. Nevertheless, because of the trend of decreasing actual with potential ET, we expect the largest leaching losses for 2011 and 2012.

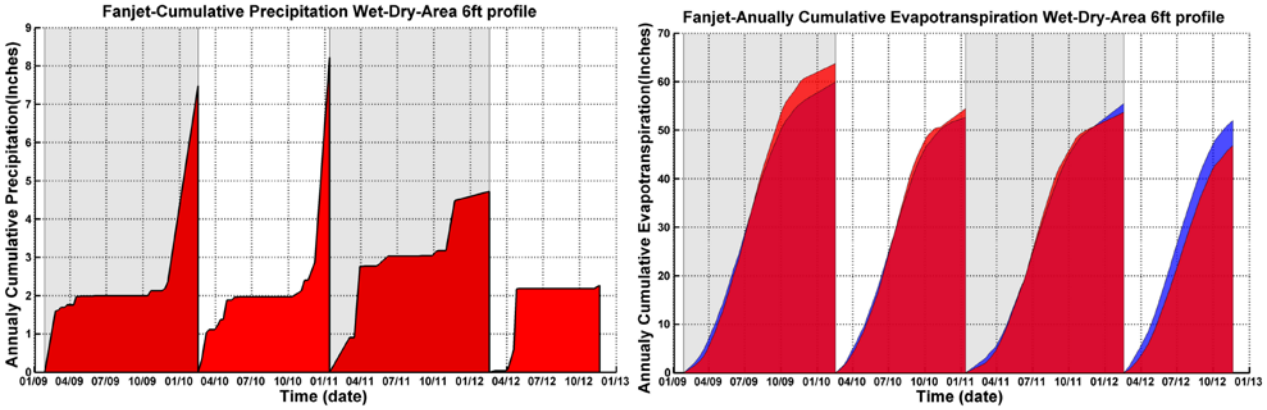

Figure 14. Annually cumulative amount of precipitation (left) and evapotranspiration (right). The precipitation (left) and the reference potential evapotranspiration (right, blue) data was obtained from a nearby CIMIS station (#146), whereas the actual crop evapotranspiration data (right, red) was computed from Eddy-Covariance data at the site.

Applied irrigation water (IW). **Figure 15** shows the cumulative amount of water applied for each year of 4 years of the 2009 – 2013 seasons for both the drip (left panel) and fanjet (right panel) sites. The amount of applied irrigation water was likely determined from change in soil profile water storage using neutron probe data. Our data show that IW for the fanjet site is lower (95%, 88%, 88%, and 90% for 2009, 2010, 2011, and 2012, respectively) than for the drip site, indicating either evaporation losses or lower than anticipated sprinkler rates for the fanjet treatment. Given the IW data, it is expected that highest leaching rates will occur for the drip site. Since both ETa and IW amounts are decreasing during the 2009-2013 period, we confirm that the irrigation scheduling was done using soil profile water depletion information.

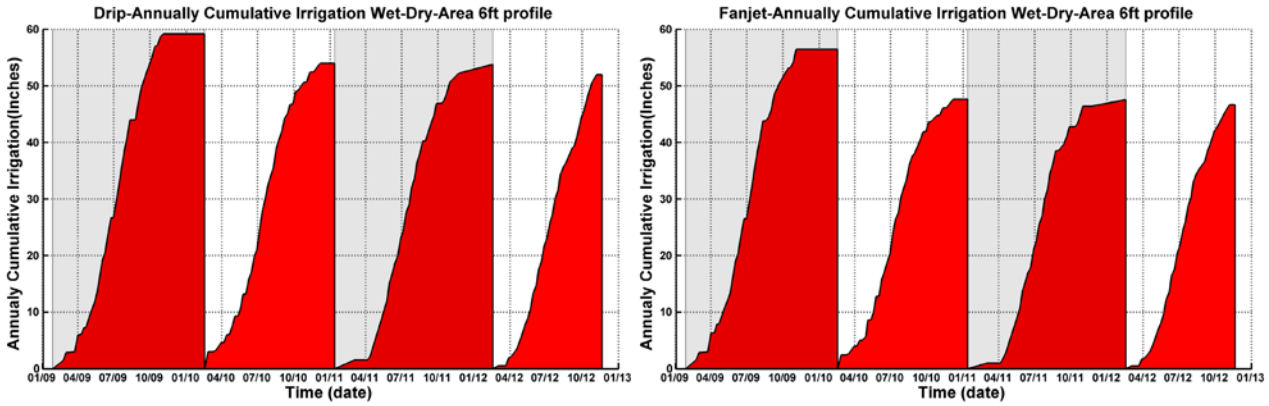

Figure 15. Annually cumulative amount of applied irrigation water in both drip (left) and fanjet (right) sites. Each plot consists of four cumulative curves of years 2009 to 2012. It is such that the amount of applied water at the beginning of each year was set to zero and total amount of applied water through each year was calculated and plotted.

Soil water storage (ΔS). The last component of the water balance equation that is required for leaching calculations is the change of soil water storage. Instead of the EchoTE measurements we used the available neutron probe data as these provided soil water content measurements down to 1.8 m.

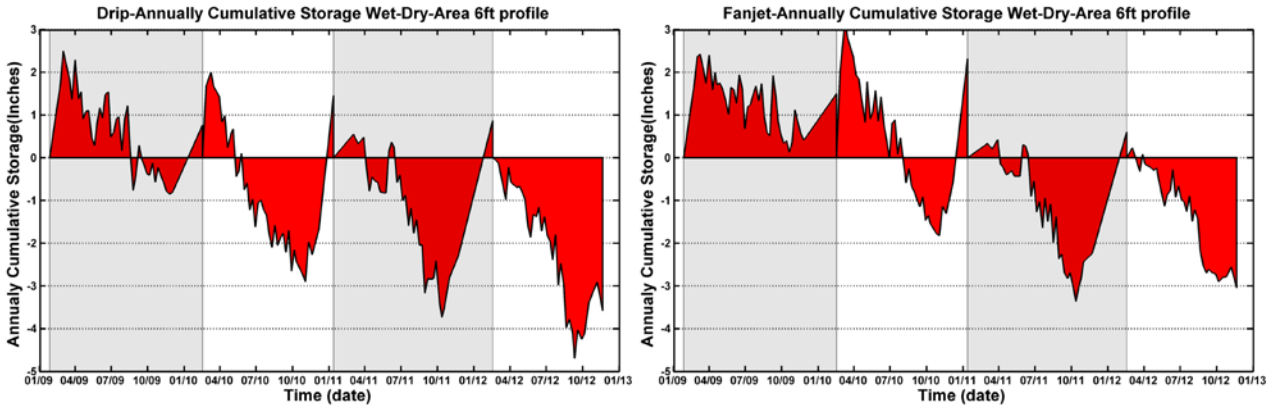

Figure 16. Cumulative amount of soil water storage for both drip (left) and fanjet (right) sites.

Figure 16 shows the cumulative storage for each year for both drip (left) and fanjet (right) sites. The presented soil water storage changes follow the same trend for both irrigation sites, with depletion cycles throughout the growing season followed by increasing soil water storage by precipitation and irrigation in the winter and spring. However, this is mostly occurring for the wetter first two years only.

Leaching rate (LR). The amount water lost through leaching can be calculated using the water balance equation [**Eq. 2**], since all other components are known. **Figure 17** presents the calculated cumulative leaching for each year (solid black line) and the uncertainty range (red area) for both drip and fanjet irrigation sites. The uncertainty was estimated, assuming a ±5% error for each component of the water balance equation. As expected, the estimated leaching amounts are higher for the last two years, because of the reduced actual ET relative to the

potential ET. However, the total leaching was significantly higher for the drip site, almost twice the magnitude for most of the last two years presented. The higher leaching for drip irrigation is expected because of two reasons. First, as shown in **Figure 15**, the amount of applied irrigation water was higher for the drip site. Second, with drip irrigation water much more locally applied (at the same irrigation rate, frequency and duration) than for the fanjet water application, it is likely that soil water storage will exceed soil water storage capacity for the soil profile of the drip site.

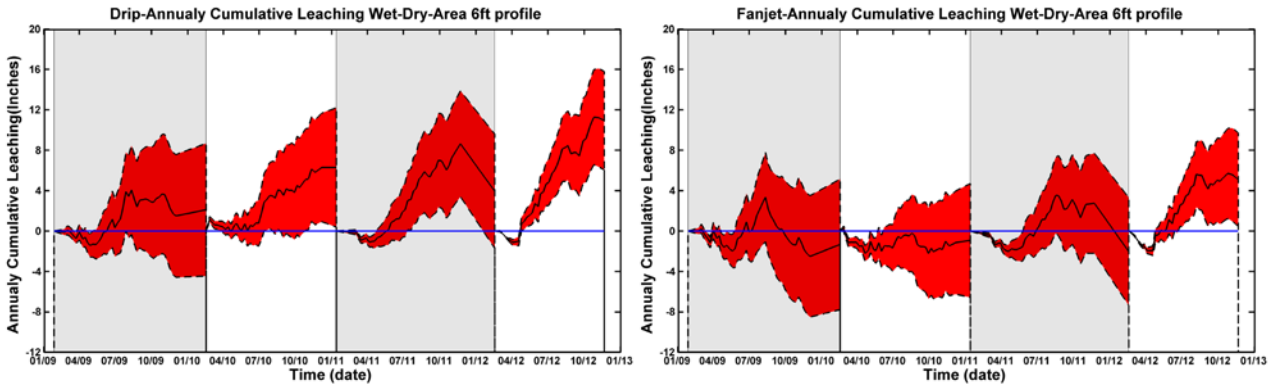

Figure 17. Cumulative amount of leaching (LR, inches) for both the drip (left) and fanjet (right) sites.

A summary of the water balance components are presented in **Table 3** below. Because the first neutron probe measurements were done between late January and mid February, the annual water balance data represent February to January data. As was already determined, the applied irrigation water in drip site was between two to six inches higher than the fanjet (F) site, thus largely causing the increased LR for the Drip (D) site, as presented by the last two rows of **Table 3** show the total amount of water leached and uncertainty range for each year. Negative and positive values represent upward flow into the soil rooting zone and downward leaching at the end of the water balance period respectively. As expected the 2012 leaching rates was significantly higher than all the other years because of this year's unusual low actual ET.

Darcy Equation. Leaching rates were computed from the Darcy equation [**Eq. 1**], considering the uncertainty in (a) soil water matric potential measurements, (b) unsaturated hydraulic conductivity curves, and (c) soil texture of the soil layers at the deep tensiometer locations. Therefore, rather than calculating single leaching rate values, we computed leaching rate uncertainty in addition. However, since the tensiometers were installed in the spring of 2012, we only report values starting May 2012.

Table 3. Summary of water balance components for all years.

		Site		Year 2009	2010	2011	2012
Water balance (inches)	IW	D		59.16	53.98	53.78	51.96
		F		56.47	47.62	47.52	46.65
	P	D/F		7.47	8.24	4.71	2.29
	ETo	D/F		59.90	52.67	55.49	52.03
	ETa	D/F		63.77	54.45	53.68	46.88
	ΔS	D		0.77	1.45	0.87	-3.60
		F		1.51	2.32	0.61	-3.06
	LR	D	Min	-4.44	0.39	-1.72	6.06
			Average	2.12	6.30	3.94	10.93
			Max	8.68	12.20	9.59	15.81
		F	Min	-7.78	-6.56	-7.36	0.45
			Average	-1.32	-0.92	-2.03	5.09
			Max	5.14	4.71	3.30	9.73

Figures 18-A and **19-A** present the average and standard deviation of matric potential values measured at the 200 and 220 cm soil depths for the drip and fanjet sites respectively. As a result of increasing root water uptake and crop transpiration from spring to summer the matric potential of the soil layer below the root zone gradually decreases (more negative) for both irrigation sites but does not increase (as a result of deep soil wetting) during the winter due to very low winter rainfall. It is shown that the deep soil matric potential slightly increased over the 2012 irrigation season but not enough to have meaningful effect on soil leaching. We note that the matric potential values of the drip site are much larger (less negative) than for the fanjet site because of either the clay layer presence at the tensiometer depth or greater amount of applied irrigation water as discussed in the previous section, or both. Moreover, the drier soil at the fanjet site is caused by reduced hydraulic conductivity of the clay layer above the 120 cm soil depth. The much larger uncertainty of the matric head values at the fanjet location is likely caused by the non-uniformity of the water application and reduced lateral spreading above the deep soil layers because of the lower water content at this site (panel B) as opposed to the drip site as caused by higher IW values.

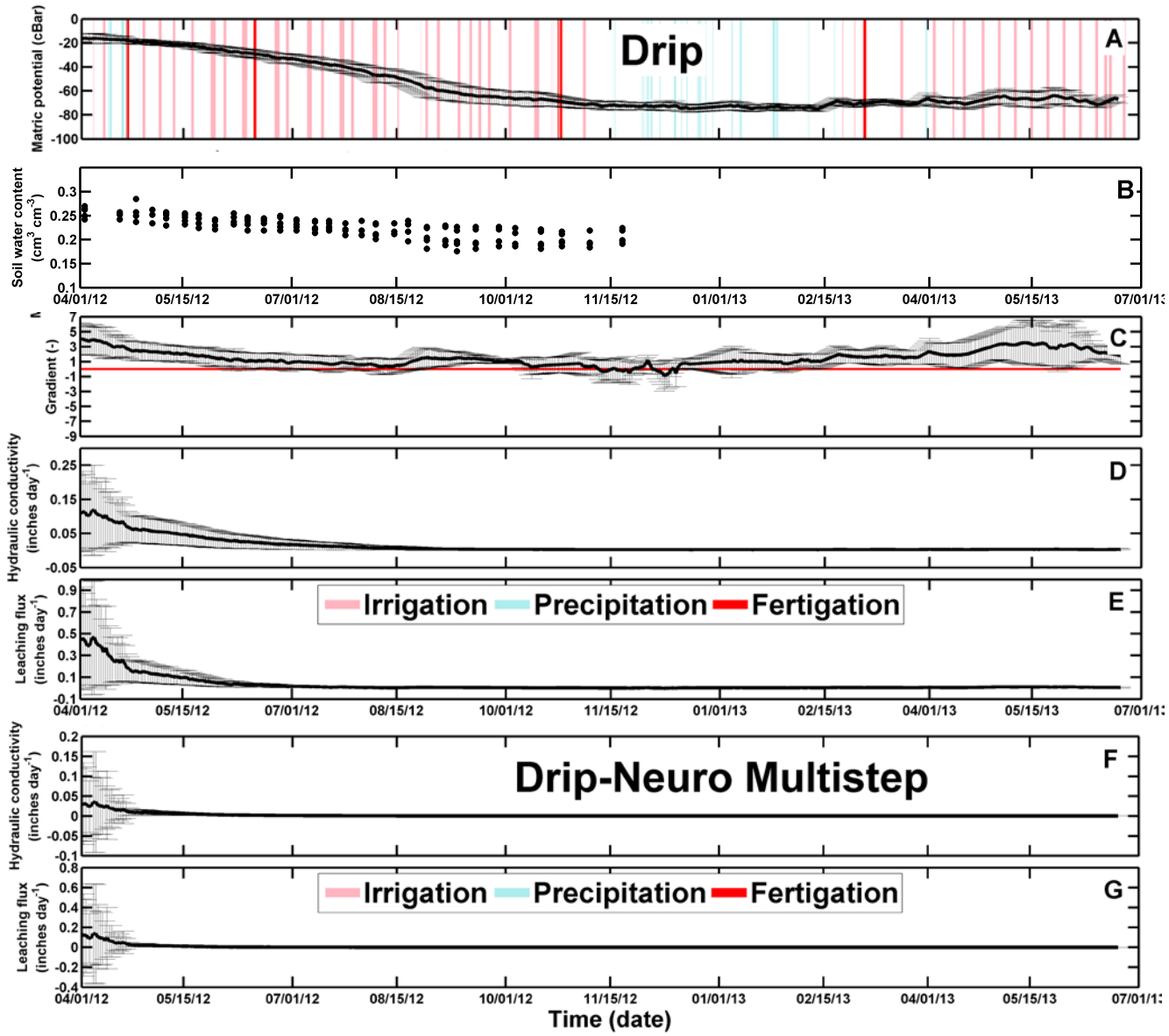

Figure 18. Spatial and temporal variations (drip) of (A) matric potential at the 200 and 220 cm soil depth, (B) deep soil water content at 210 cm, (C) total head gradient, (D and F) unsaturated hydraulic conductivity for multistep and Neuro Multistep methods respectively, and (E and G) leaching rate for multistep and Neuro Multistep methods respectively as measured for 4 locations (**Figure 1**) starting April 1, 2012 through July 1, 2013. Average values are presented by the thick black lines whereas the spatial variations are presented by the error bars, defined by standard deviations (error bars). The pink, blue, and red bars represent irrigation, precipitation, and fertigation events respectively.

Figures 18-B and **19-B** shows the temporal variation of soil water content measured at the 210 cm soil depth from neutron probe measurements. The general higher water content values for the drip site correspond with the general less negative soil matric potential values presented in **Figures 18-A** and **19-A.** From the measured matric head values at the 200 and 220 cm soil depths, the total head gradient with corresponding spatial variations (standard deviation values) are plotted in **Figures 18-C and 19-C**. Typically, average total head

gradients in fanjet site vary between 2 and 4, indicating downward soil water flow, but gradually decreasing

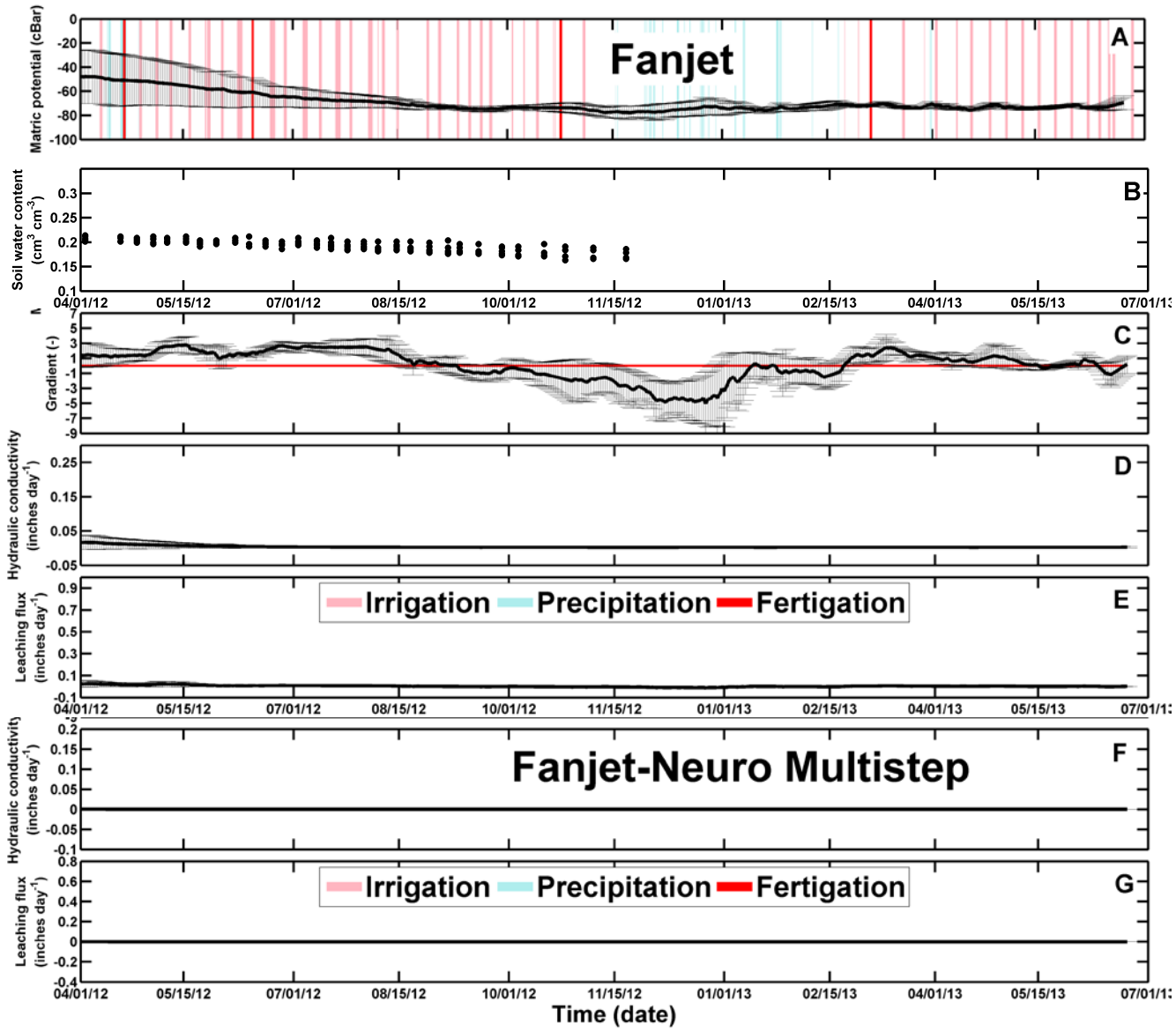

Figure 19. Spatial and temporal variations (Fanjet) of (A) matric potential at the 200 and 220 cm soil depth, (B) deep soil moisture at 220 cm, (C) total head gradient, (D and F) unsaturated hydraulic conductivity for multistep and Neuro Multistep methods respectively, and (E and G) leaching rate for multistep and Neuro Multistep methods respectively as measured for 4 locations (**Figure 1**) starting April 1, 2012 through July 1, 2013. Average values are presented by the thick black lines whereas the spatial variations are presented by the error bars, defined by standard deviations (error bars). The pink, blue, and red bars represent irrigation, precipitation, and fertigation events respectively.

through the summer and fall, reaching negative total head gradients of 3 to 7 resulting in upwards capillary flow into the tree root zone. This negative gradient increased through the winter reaching the unit gradient for the 2013 growing season period. The same trend is shown for the drip site (**Figure 18-C**). Variations are typically large and are caused by uncertainty in tensiometer readings and soil heterogeneity.

In order to compute the leaching rate at the 200-220 cm soil depth, we need to substitute the unsaturated hydraulic conductivity value of this layer in **Eq. 1**, which is dependent on soil texture and soil water matric potential at the tensiometer locations. However, because of the large variations in both matric potential and soil texture we present the range in unsaturated hydraulic conductivity (**Figures 18D** and **19D**) as determined from the uncertainty ranges of matric potential (**Figures 18-A** and **19-A**) and unsaturated hydraulic conductivity curves (**Figure 9b**). The latter is controlled by soil texture but is partly unknown because of the apparent high spatial variability of soil texture and soil layering. It is therefore that we calculated the unsaturated hydraulic conductivity of all the soil types for the given range of matric potential as presented by the filled-in areas in **Figure 9b.** The much higher unsaturated hydraulic conductivity values for the drip site is a result of the higher soil water matric potential (compare **Figure 18- A** with **Figure 19-A**) at the 200 cm depth. Despite the large variation in matric potential for the fanjet, the corresponding uncertainty range for the hydraulic conductivity is smaller than for the drip site and is a result of the much lower matric potential (more negative) for the fanjet site. The final estimated leaching rate values are presented in **Figures 18-E** and **19-E** showing that both the average and variation of the leaching rates is much higher for the drip site than for the fanjet site with mean leaching rate values ranging between 0-0.4 in/day (drip) and 0-0.02 in/day (fanjet). We believe that the much lower leaching rates for the fanjet site is mainly caused by lower amount of applied irrigation water and to some extent due to the impeding clay layer at the 120 cm depth.

In addition to computing leaching rates from the measured unsaturated hydraulic conductivity curves, we include in **Figures 18-F** and **19-F** the predicted hydraulic conductivity curves and associate uncertainty using the Neuro Multistep results of **Figure 10**. As the results indicate, the predicted hydraulic conductivities (panels **F**) are close to the measured values for the wet soil conditions in the spring of 2012, but are much lower as soil water content decreases in the late spring. **Figures 18-G** and **19-G** show the leaching rates calculated using the hydraulic conductivities estimated by the neural network model. As expected, the mean leaching rate values for the drip site are higher than for the fanjet site because of soil water content differences discussed before.

Comparison of LR between water balance and Darcy equation approaches. Table 4 shows a comparison between leaching rates estimated using the water balance approach with the Darcy equation approach, presenting both measured and predicted unsaturated hydraulic conductivity curves. We note that the estimated uncertainty is significantly larger for the Darcy calculations but in general annual total LR values are reasonably close between the two methods.

Table 4. Comparison of LR and uncertainty range from water balance and Darcy equation approaches.

			Water balance	Darcy-Multistep K(h)	Darcy-Neuro Multistep K(h)
Leaching (inches)	Drip	Min	7.27	2.59	0.18
		Average	11.9	12.91	2.32
		Max	16.51	48.97	48.47
	Fanjet	Min	2.22	0.1	0
		Average	6.59	1.43	0.03
		Max	10.96	6.39	0.11

This huge uncertainty, especially for the drip site, comes from the uncertainty of the soil hydraulic conductivity curves. Comparing the uncertainty range between drip and fanjet, one could conclude that the main uncertainty come from unknown unsaturated conductivity, especially in the wet end, because LR values tend to be near zero in the dry water content range. We believe that inverse modeling, using HYDRUS and in-situ soil moisture, and water potential data could be a realistically better approach to determine the soil hydraulic properties in the future.

Soil electrical conductivity and nitrate concentration measurements. Figure 20 shows the temporal variations of soil electrical conductivity (EC) at different depths in both fanjet and drip sites as determined by Blake Sanden. These soil salinity data confirm our hypothesis that the leaching rates are controlled mainly by the amount of applied irrigation water and also by the most shallow clay layer within the soil profile (as represented by the gray bands in **Figure 21**). The lower leaching rates cause higher soil salinity in the soil profile of the fanjet site.

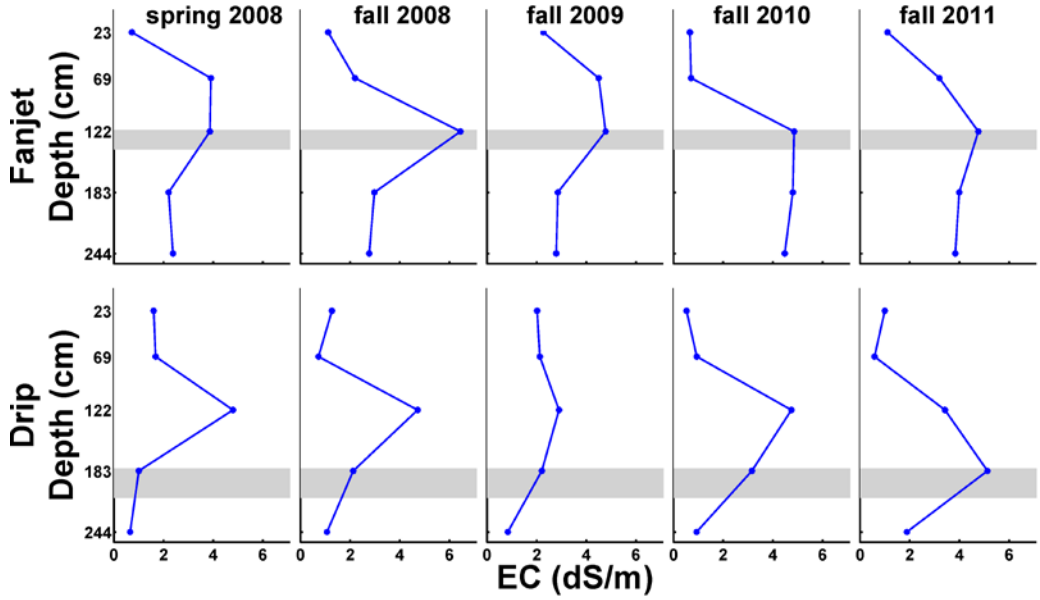

Figure 20. Temporal variations of soil electrical conductivity (EC) at different depth in both fanjet and drip sites. The horizontal gray bar represents the clay layer. Data provided by Blake Sanden.

Figures 21 and **22** show the temporal variations of soil nitrate concentration at different depths (each row of subplots represents different depth) for a series of days after each fertigation. The soil nitrate mass is at minimum before fertigation, then increases to a maximum immediately after fertigation and gradually decreases as nutrient is taken up by tree root uptake or leaches downwards. Much of the lack of soil nitrate solution data are attributed to later installation of solution samplers at the larger soil depths, and inability to extract soil solution because of too dry soil conditions (especially for fanjet site). Spatial variations in nitrate concentration are caused by non-uniform water and associated nutrient applications, non-uniform root nutrient uptake, and spatial variations in soil water content.

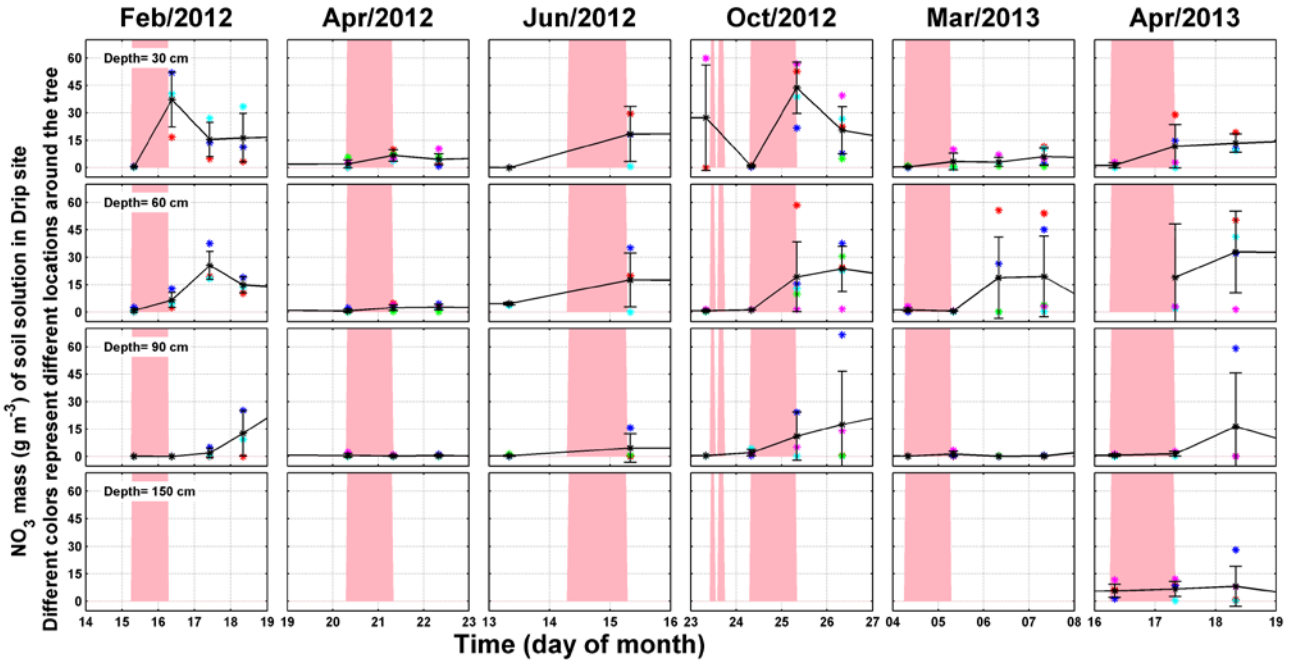

Figure 21. Temporal variations of soil nitrate mass (g m^{-3}) at different depths in **drip** site after each fertigation. Different colored points represent different location around the tree. The pink bar shows the period of fertigation event.

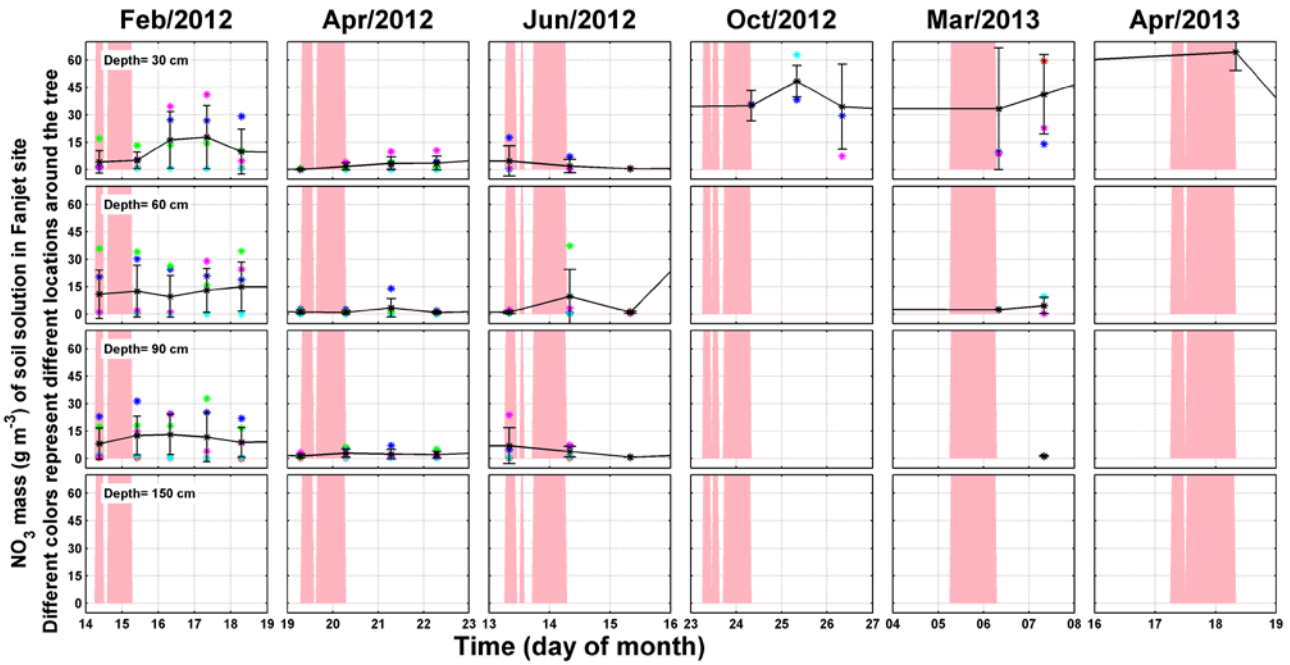

Figure 22. Temporal variations of soil nitrate mass (g m^{-3}) at different depths in **fanjet** site after each fertigation. Different colored points represent different locations around the tree. The pink bar shows the period of the fertigation event.

To date the nitrate measurements show that there is no general change in soil nitrate storage between fertigations, indicating that all applied nitrate is either taken up or lost by leaching/denitrification. Although not shown here, nitrate losses by denitrification are generally very low and are less than one percent of the total applied nitrate (David Smart lab at UC Davis). With leaching rates determined to be near zero for most of the growing season, we can therefore assume that most of the applied nitrate is taken up by the almond crop, except for the early spring period when the soil is wet and leaching occurs. In the coming year, we will combine the soil nitrate data with applied nitrate and biomass nitrate information and complete a total nitrate mass balance for both sites. Tentatively though our data suggest that nitrate losses are likely to occur only in the winter and spring period when the soil is wet and root water uptake rates are relatively low.

Research Effort Recent Publications:

Hopmans, J.W., M.M. Kandelous, A. Olivos, B.R. Hanson and P. Brown. 2010. Optimization of water use and nitrate use for almonds under micro-irrigation. Almond Industry Conference, Modesto, CA.

Hopmans J.W., and M. M. Kandelous. 2013. How does Nitrogen move in the soil, and what are the factos that influence its movement. Citrograph, May/June 2013, pages 22-28.

Kandelous, M.M, T. Kamai, J.A. Vrugt, J. Simunek, B.R. Hanson and J.W. Hopmans. 2010. An optimization model to design and manage subsurface drip irrigation system for alfalfa. AGU Fall meeting, San Francisco, CA.

Kandelous, M.M, A. Olivos, P. Brown, and J.W. Hopmans, 2011. Optimization of water use and nitrate use for almonds under micro-irrigation. Almond Industry Conference, Modesto, CA.

Kandelous, M.M., Moradi, A.B., Hopmans, J.W., Burger, M., 2012. coupled experimental-modeling approach for estimation of root zone leaching of applied irrigation water and fertilizers, AGU Fall Meeting. AGU, San Francisco.

Kandelous, M.M, A. Olivos, P. Brown, and J.W. Hopmans, 2012. Optimization of water use and nitrate use for almonds under micro-irrigation. Almond Industry Conference, Sacramento, CA.

Kandelous M.M., T. Kamai, J.A. Vrugt, J. Simunek, B.R. Hanson, and J.W. Hopmans. 2012. Evaluation of subsurface drip irrigation design and management parameters for alfalfa. Agric. Water Management. Doi:10.1016/j.agwat.2012.02.009

References Cited:

Minasny, B., J.W. Hopmans, T.H. Harter. A.M. Tuli. S.O. Eching and D.A. Denton. 2004. Neural network prediction of soil hydraulic functions for alluvial soils using multi-step outflow data. Soil Science Soc. Amer. J. 68:417-429.

Tuli, A., M. A. Denton, J. W. Hopmans, T. Harter, and J. L. Mac Intyre. 2001. Multi-step outflow experiment: From soil preparation to parameter estimation. LAWR Rep. 100037 (http://researchers.lawr.ucdavis.edu/tuli/REPRINTS/MULTISTEPOUTFLOW.pdf)